Front. Phys. 11(3), 117201 (2016)
DOI 10.1007/s11467-016-0566-5

RESEARCH ARTICLE

Thermoelectric response of spin polarization in Rashba spintronic systems

Cong Xiao, Dingping Li†, Zhongshui Ma

School of Physics, Peking University, Beijing 100871, China
Collaborative Innovation Center of Quantum Matter, Beijing 100871, China
Corresponding author. E-mail: †lidp@pku.edu.cn

Received January 24, 2016; accepted February 4, 2016

Motivated by the recent discovery of a strongly spin–orbit-coupled two-dimensional (2D) electron gas near the surface of Rashba semiconductors BiTeX (X = Cl, Br, I), we calculate the thermoelectric responses of spin polarization in a 2D Rashba model. By self-consistently determining the energy- and band-dependent transport time, we present an exact solution of the linearized Boltzmann equation for elastic scattering. Using this solution, we find a non-Edelstein electric-field-induced spin polarization that is linear in the Fermi energy E_F when E_F lies below the band crossing point. The spin polarization efficiency, which is the electric-field-induced spin polarization divided by the driven electric current, increases for smaller E_F. We show that, as a function of E_F, the temperature-gradient-induced spin polarization increases continuously to a saturation value when E_F decreases below the band crossing point. As the temperature tends to zero, the temperature-gradient-induced spin polarization vanishes.

Keywords thermoelectric response, spin polarization, Rashba spin–orbit coupling, Boltzmann equation, analytical solution

PACS numbers 72.25.Dc, 79.10.-n, 75.76.+j, 72.25.Rb

1 Introduction

Two-dimensional electron systems (2DESs) with spin–orbit coupling (SOC) show many fascinating transport phenomena due to mixing of the spin and orbital degrees of freedom, providing the possibility of realizing all-electrical and all-thermal spin control in semiconductor structures. These are the main topics of the rapid developing research fields of spintronics [1, 2] and spin caloritronics [3, 4]. In electrical spin control, the generation of a spin current and a nonequilibrium spin polarization transverse to an applied electric field without an external magnetic field are remarkable; these phenomena are known as the spin Hall effect [5, 6] and electric-field-induced spin polarization (EISP) [7–9], respectively. Their thermal counterparts toward all-thermal spin control, i.e., the spin Nernst effect [10–14] and temperature-gradient-induced spin polarization (TISP) [15–17], have also attracted increasing interest recently.

The 2DES with Rashba SOC has been among the models most widely used to investigate these effects [10, 12, 15, 16]. In the 2D Rashba model, two bands cross at zero energy; one of them is always positive, and the other possesses a band valley regime below the band crossing point, as shown in Fig. 1. In this valley regime, the dispersion curve is not monotonic in momentum space. This regime possesses a nontrivial topology of the constant energy surfaces (or Fermi surfaces) [18], which leads to some exciting theoretical predictions, e.g., an enhanced superconducting critical temperature [18], non-Dyakonov–Perel spin relaxation behavior [19], and a significantly enhanced room-temperature thermoelectric figure of merit [20]. There have been a few theoretical studies [16, 19–22] of the transport properties when the Fermi energy is in or near the band valley regime. However, in Rashba systems formed in conventional narrow-gap semiconductor heterostructures [23], the Rashba spin splitting energy is so small that the band valley structure cannot survive weak disorder broadening and thermal smearing, even at very low temperatures. In these systems, the Fermi energy usually lies well above the band crossing point; therefore, the band valley is irrelevant to transport.

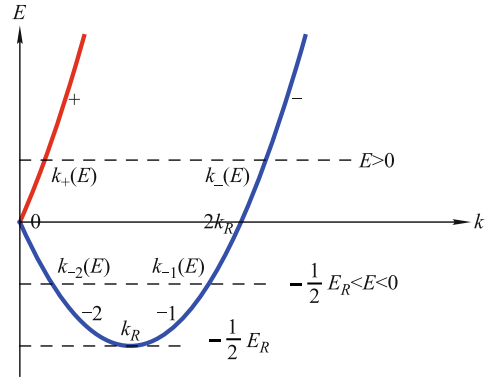

Fig. 1 Band structure of the 2D Rashba system. The energy of the band crossing point is chosen to be zero. The wave number and energy of the bottom of the dispersion curve is k_R and $-\frac{1}{2}E_R$, respectively. Corresponding to a given energy $E \geqslant 0$, the wave number in $\pm$ band is denoted by $k_\pm(E)$. For $-\frac{1}{2}E_R < E \leqslant 0$, there are two monotonic regimes on $E-k$ curve: the one from $k=0$ to k_R is marked by the branch -2, whereas the other from $k=k_R$ to $2k_R$ marked by branch -1. The wave number $k_{-\nu}(E)$ represents the wave number in the $-\nu$ branch at given E, where $\nu = 1, 2$.

Experimental progress has been made recently with the discovery of giant bulk and surface Rashba SOC effects in V-VI-VII polar semiconductors BiTeX (X = Cl, Br, I) [24–28]. In these noncentrosymmetric semiconductors, first-principles calculations and angle-resolved photoemission spectroscopy measurements have clearly demonstrated the existence of a 2DES confined near the surface with a giant Rashba energy as large as about 10^2 meV [29, 30]. The investigation of electrical and thermal spin control in such a 2DES is important because of the giant SOC, which is promising for spintronics and spin caloritronics applications. However, when electron–impurity scattering dominates, the giant Rashba SOC invalidates the relaxation time approximation (RTA) used in previous theoretical works on nonequilibrium spin polarization [16, 22] if the Fermi energy lies below or near the band crossing point. This motivates us to systematically investigate the thermoelectric response of spin polarization in 2DESs with giant Rashba SOC, focusing on the consequences of different Fermi surface topologies on either side of the band crossing point.

In this paper, we employ the semiclassical Boltzmann equation (SBE) to calculate the spin polarization induced by an electric field or a temperature gradient. We focus on the 2D Rashba model at low temperatures, where static impurity scattering dominates. Our calculation is based on an exact transport time solution of the Boltzmann equation in the Born approximation, which differs from the widely used modified RTA [31] and the constant RTA [16, 20, 22]. We show that the EISP as a function of the Fermi energy E_F behaves differently on either side of the band crossing point $E_F = 0$. A linear dependence of the EISP on E_F is obtained for $E_F < 0$, which differs from the Edelstein result [7] for $E_F \geqslant 0$. The spin polarization efficiency, defined as the ratio between the EISP and the driven electric current, increases for lower E_F. The TISP is calculated, and its dependence on the Fermi energy which changes from large positive values to well below the band crossing point, is continuous and monotonic. It is also shown that the TISP tends to zero at vanishing temperature.

The paper is organized as follows. We present the model and the semiclassical Boltzmann formalism in Section 2, and the exact solution of the SBE is given in Section 3. The analytical and numerical results for the EISP and TISP are shown in Section 4. Finally, we conclude this paper in Section 5. The technical details of the solution of the SBE are presented in Appendixes A and B.

2 Semiclassical Boltzmann descriptions of thermoelectric spin responses in a 2D Rashba spintronic system

2.1 Basic solutions for the 2D Rashba model

We study the 2D Rashba model with spin-independent disorder

$$H = \frac{\boldsymbol{p}^2}{2m} + \frac{\alpha}{\hbar}\boldsymbol{\sigma}\cdot(\boldsymbol{p}\times\hat{\boldsymbol{z}}) + V(\boldsymbol{r}), \tag{1}$$

where $V(\boldsymbol{r}) = \sum_i V_i\delta(\boldsymbol{r}-\boldsymbol{R}_i)$ is the disorder potential produced by randomly distributed δ-scatters at $\boldsymbol{R}_i$ and is assumed to be standard white-noise disorder: $\langle|V_{\boldsymbol{k}'\boldsymbol{k}}|^2\rangle_{dis} = n_{im}V_0^2$. Here n_{im} is the impurity concentration, $V_{\boldsymbol{k}'\boldsymbol{k}}$ is the spin-independent part of the disorder matrix element, and $\langle\ldots\rangle_{dis}$ is the average over disorder configurations. Further, m is the in-plane effective mass of the conduction electron, $\boldsymbol{p} = \hbar\boldsymbol{k}$ is the momentum, $\boldsymbol{\sigma} = (\sigma_x, \sigma_y, \sigma_z)$ are the Pauli matrices, and α is the Rashba coefficient. The eigenenergies of the pure system are $E_{\lambda k} = \frac{\hbar^2k^2}{2m} + \lambda\alpha k$, and the inner eigenstates are $|u_{\lambda\boldsymbol{k}}\rangle = \frac{1}{\sqrt{2}}[1, -\mathrm{i}\lambda\exp(\mathrm{i}\phi)]^T$, where $\lambda = \pm$ and $\tan\phi = k_y/k_x$. The wave number at a given energy $(E > 0)$ in the λ band is given as $k_\lambda(E) = -\lambda k_R + \frac{1}{\alpha}\sqrt{E_R^2 + 2E_RE}$ (see Fig. 1), where we define the Rashba energy as $E_R = m\left(\frac{\alpha}{\hbar}\right)^2$, and $k_R = \frac{E_R}{\alpha}$. The density of states (DOS) at a given $E \geqslant 0$ is given by $N_>(E) = \sum_\lambda N_\lambda(E)$, where

$$N_\lambda(E) = N_0\frac{k_\lambda(E)}{k_\lambda(E)+\lambda k_R}. \tag{2}$$

Here $N_0 = \frac{m}{2\pi\hbar^2}$. For $E > 0$, the group velocity and

intraband spin matrix element are given by

$$\boldsymbol{v}(E,\lambda,\phi)=\frac{N_0}{N_\lambda(E)}\frac{\hbar\boldsymbol{k}_\lambda(E)}{m} \tag{3}$$

and

$$\langle u_{\lambda\boldsymbol{k}_\lambda(E)}|\boldsymbol{\sigma}|u_{\lambda\boldsymbol{k}_\lambda(E)}\rangle=\lambda(\sin\phi\hat{\boldsymbol{x}}-\cos\phi\hat{\boldsymbol{y}}), \tag{4}$$

respectively.

The direction of the group velocity is the same as that of the corresponding momentum because of the isotropic band structure and the monotonic $E-k$ curve when $E\geqslant 0$. The directions of the spin in the two bands at the same polar angle ϕ are opposite to each other.

The lower band has a valley centered at k_R, and the DOS is one-dimensional in the $E_-(k_R)\leqslant E<0$ regime [18], where $E_-(k_R)=-\frac{1}{2}E_R$ is the energy at the bottom of the dispersion curve. For $E_-(k_R)<E<0$, there are two wave numbers, $k_{-2}(E)<k_R<k_{-1}(E)$, with $k_{-\nu}(E)=k_R+(-1)^{\nu-1}\frac{1}{\alpha}\sqrt{E_R^2+2EE_R}$, where $-\nu=-1,-2$ denotes the two monotonic branches in this energy regime (see Fig. 1). The DOS $N_<(E)$ in the band valley regime is given by $N_<(E)=\sum_{\nu=1}^{2}N_{-\nu}(E)$, where

$$N_{-\nu}(E)=N_0\frac{k_{-\nu}(E)}{|k_{-\nu}(E)-k_R|}. \tag{5}$$

For $E_-(k_R)<E<0$, one obtains

$$\langle u_{-\boldsymbol{k}_{-\nu}(E)}|\boldsymbol{\sigma}|u_{-\boldsymbol{k}_{-\nu}(E)}\rangle=-\sin\phi\hat{\boldsymbol{x}}+\cos\phi\hat{\boldsymbol{y}} \tag{6}$$

and

$$\boldsymbol{v}(E,-\nu,\phi)=(-1)^{\nu-1}\frac{N_0}{N_{-\nu}(E)}\frac{\hbar\boldsymbol{k}_{-\nu}(E)}{m}. \tag{7}$$

The direction of the group velocity is parallel (antiparallel) to the corresponding momentum in the $-\nu=-1$ (-2) branch, respectively, because of the nonmonotonic $E-k$ curve in the band valley regime. The directions of the spin in the two monotonic branches at the same ϕ are the same. These characteristics show different spin and group-velocity textures of constant-energy circles between the two energy regimes on either side of the band crossing point.

Exactly at the band crossing point $(E,k)=(0,0)$, the eigenstate as well as the group velocity and spin matrix element are not well-defined because the polar angle ϕ is arbitrary. However, this does not affect the physical quantities because the DOS at this point is zero, as shown in Eqs. (2) and (5).

2.2 General formula of spin polarization in response to external fields

The out-of-equilibrium spin density response to external fields can be obtained in the semiclassical version of linear response theory and can be decomposed into intrinsic and extrinsic components:

$$\langle\hat{\boldsymbol{\sigma}}\rangle\equiv\langle\hat{\boldsymbol{\sigma}}\rangle_{int}+\langle\hat{\boldsymbol{\sigma}}\rangle_{ext}, \tag{8}$$

where

$$\begin{aligned}\langle\hat{\boldsymbol{\sigma}}\rangle_{int}&=\sum_l f_l^0 2Re\langle\psi_l^{(0)}|\boldsymbol{\sigma}|\delta\psi_l\rangle,\\ \langle\hat{\boldsymbol{\sigma}}\rangle_{ext}&=\sum_l g_l\langle\psi_l^{(0)}|\boldsymbol{\sigma}|\psi_l^{(0)}\rangle.\end{aligned} \tag{9}$$

Here f_l^0 is the equilibrium Fermi–Dirac distribution function (DF), g_l denotes the out-of-equilibrium change in the DF, and $l=(\lambda,\boldsymbol{k})$ is the eigenstate index denoting the band and momentum. $|\psi_l^{(0)}\rangle$ is the eigenstate of the disorder-free Hamiltonian in the absence of external fields, and $|\delta\psi_l\rangle$ describes the virtual interband transition induced by weak external fields.

$\langle\hat{\boldsymbol{\sigma}}\rangle_{int}$ represents the spin density response resulting from an intrinsic mechanism based solely on the spin–orbit-coupled band structure. It is not difficult to verify that $\langle\hat{\boldsymbol{\sigma}}\rangle_{int}=0$ for the present model, so one needs only to analyze the extrinsic spin density response $\langle\hat{\boldsymbol{\sigma}}\rangle_{ext}$, which depends on the existence of disorder via g_l.

The SBE can be used to calculate g_l in the presence of a uniform weak electric field and small chemical potential and temperature gradients in nonequilibrium steady states. Here we consider low temperatures, where static impurity scattering dominates the electron relaxation. The Boltzmann equation reads

$$\boldsymbol{F}_l\cdot\boldsymbol{v}_l\frac{\partial f^0}{\partial E_l}=-\sum_{l'}w_{l',l}[g_l-g_{l'}], \tag{10}$$

where the generalized force acting on the state l is $\boldsymbol{F}_l=-\frac{E_l-\mu}{T}\boldsymbol{\nabla}T-\boldsymbol{\nabla}\mu+e\boldsymbol{E}$, and $\boldsymbol{E}$, μ, and T are the electric field, chemical potential, and absolute temperature, respectively. Further, $w_{l',l}$ is the transition rate from state l' to l, which can be determined by the golden rule in single-particle quantum mechanical scattering theory. In the present system without the anomalous Hall effect, the lowest-order Born approximation is sufficient [32]:

$$w_{l',l}=\frac{1}{\tau_0 N_0}|\langle u_{l'}|u_l\rangle|^2\delta(E_l-E_{l'}), \tag{11}$$

where $\tau_0=\left(\frac{2\pi n_{im}V_0^2N_0}{\hbar}\right)^{-1}$. When $E>0$, the intraband and interband elastic scattering can be represented by $\omega_{\lambda',\lambda}(E=E_l)=\int\mathrm{d}E_{l'}w_{l',l}$:

$$\omega_{\lambda',\lambda}(E)=\frac{1}{\tau_0 N_0}\frac{1}{2}[1+\lambda\lambda'\cos(\phi'-\phi)]. \tag{12}$$

For $E_-(k_R)<E<0$, we introduce $\omega_{-\nu',-\nu}(E=E_l)=$

$\int \mathrm{d}E_{l'} w_{l',l}$ to represent intrabranch and interbranch scattering:

$$\omega_{-\nu',-\nu}(E) = \frac{1}{\tau_0 N_0}\frac{1}{2}[1+\cos(\phi'-\phi)]. \tag{13}$$

3 Exact solution of the SBE

In this section, we analytically solve the SBE on the basis of the isotropic transport times. For $E > 0$, the Boltzmann equation includes both direct intraband and interband elastic scattering, whereas for $E_-(k_R) < E < 0$, only intraband scattering in the lower band occurs. Because of the band valley structure below the band crossing point, the solution in this regime is nontrivial and differs completely from that in ordinary single-band cases. Finally, we clearly show that for positive and negative energies, the DFs are formally similar.

3.1 Exact solution of the SBE for $E > 0$

When $E > 0$, the SBE can be re-expressed as

$$\begin{aligned}&\boldsymbol{F}_E \cdot \boldsymbol{v}(E,\lambda,\phi)\frac{\partial f^0}{\partial E}\\ &= -\sum_{\lambda'} N_{\lambda'}(E)\int \frac{\mathrm{d}\phi'}{2\pi}\omega_{\lambda',\lambda}(E)\\ &\quad\times[g_\lambda(E,\vartheta(\boldsymbol{v}(E,\lambda,\phi)))\\ &\quad -g_{\lambda'}(E,\vartheta(\boldsymbol{v}(E,\lambda',\phi')))],\end{aligned} \tag{14}$$

where $\vartheta(\boldsymbol{v}(E,\lambda,\phi))$ denotes the angle of the direction of $\boldsymbol{v}(E,\lambda,\phi)$ with respect to the direction of the applied generalized force $\boldsymbol{F}_E = -\frac{E-\mu}{T}\boldsymbol{\nabla}T - \boldsymbol{\nabla}\mu + e\boldsymbol{E}$. According to Eq. (3), $\vartheta(\boldsymbol{v}(E,\lambda,\phi)) = \vartheta(\boldsymbol{k}_\lambda(E))$. The above SBE can be solved by introducing the isotropic transport time for electrons with energy E in the λ band as

$$g_\lambda(E,\vartheta(\boldsymbol{k}_\lambda(E))) = \left(-\frac{\partial f^0}{\partial E}\right)\boldsymbol{F}_E\cdot\boldsymbol{v}(E,\lambda,\phi)\tau_\lambda(E), \tag{15}$$

and the transport time is determined self-consistently by substituting Eq. (15) into Eq. (14). Thus, we obtain (details in Appendix A)

$$\begin{aligned}\frac{1}{\tau_\lambda(E)} &= \sum_{\lambda'} N_{\lambda'}(E)\int\frac{\mathrm{d}\phi'}{2\pi}\omega_{\lambda',\lambda}(E)\\ &\quad\times\left[1-\frac{|\boldsymbol{v}(E,\lambda',\phi')|}{|\boldsymbol{v}(E,\lambda,\phi)|}\cos(\phi'-\phi)\frac{\tau_{\lambda'}(E)}{\tau_\lambda(E)}\right],\end{aligned} \tag{16}$$

the solution of which is

$$\tau_\lambda(E) = \tau_0\frac{N_\lambda(E)}{N_0}\left(\frac{2N_0}{N_>(E)}\right)^2, \tag{17}$$

where $N_>(E) = 2N_0$.

When this solution is combined with Eq. (4), the out-of-equilibrium DF has the compact form

$$g_\lambda\left(E,\vartheta\left(\boldsymbol{k}_\lambda(E)\right)\right) = \left(-\frac{\partial f^0}{\partial E}\right)\boldsymbol{F}_E\cdot\frac{\hbar\boldsymbol{k}_\lambda(E)}{m}\tau_0, \tag{18}$$

which satisfies the particle number conservation requirement

$$\sum_\lambda\int \mathrm{d}E N_\lambda(E)\int\frac{\mathrm{d}\phi}{2\pi}g_\lambda\left(E,\vartheta\left(\boldsymbol{k}_\lambda(E)\right)\right) = 0. \tag{19}$$

Equation (18) resembles the DF for a spin-degenerate free electron gas without SOC [29], but the important difference is that in the present case, the group velocity is given by Eq. (4) rather than $\frac{\hbar\boldsymbol{k}_\lambda(E)}{m}$ for positive energies.

3.2 Exact solution of the SBE for $E_-(k_R) < E < 0$

Now we come to the energy regime $E_-(k_R) < E < 0$. By converting the momentum integration in Eq. (10) into energy integration and noticing the directions of the group velocity in the two monotonic branches, the SBE can be re-expressed as (details in Appendix B)

$$\begin{aligned}&\boldsymbol{F}_E\cdot\boldsymbol{v}(E,-\nu,\phi)\frac{\partial f^0}{\partial E}\\ &= -\sum_{\nu'}N_{-\nu'}(E)\int\frac{d\phi'}{2\pi}\omega_{-\nu',-\nu}(E)\\ &\quad\times[g_{-\nu}(E,\vartheta(\boldsymbol{v}(E,-\nu,\phi)))\\ &\quad -g_{-\nu'}(E,\vartheta(\boldsymbol{v}(E,-\nu',\phi')))],\end{aligned} \tag{20}$$

which is similar to Eq. (14) for $E > 0$.

The derivation of the transport time solution of Eq. (20) is similar to that for $E > 0$. Substituting

$$\begin{aligned}&g_{-\nu}(E,\vartheta(\boldsymbol{v}(E,-\nu,\phi)))\\ &\quad= \left(-\frac{\partial f^0}{\partial E}\right)\boldsymbol{F}_E\cdot\boldsymbol{v}(E,-\nu,\phi)\tau_{-\nu}(E)\end{aligned} \tag{21}$$

into Eq. (20), we obtain the following self-consistent equation for $\tau_{-\nu}$:

$$\begin{aligned}\frac{1}{\tau_{-\nu}(E)} &= \sum_{\nu'}N_{-\nu'}(E)\int\frac{\mathrm{d}\phi'}{2\pi}\omega_{-\nu',-\nu}(E)\\ &\quad\times\left[1-\frac{|\boldsymbol{v}(E,-\nu',\phi')|}{|\boldsymbol{v}(E,-\nu,\phi)|}\frac{\cos\vartheta(\boldsymbol{v}(E,-\nu',\phi'))}{\cos\vartheta(\boldsymbol{v}(E,-\nu,\phi))}\frac{\tau_{-\nu'}(E)}{\tau_{-\nu}(E)}\right].\end{aligned} \tag{22}$$

Because the direction of the group velocity can be parallel or antiparallel to that of the momentum, i.e., $\vartheta(\boldsymbol{v}(E,-1,\phi)) = \vartheta(\boldsymbol{k}_{-1}(E))$, $\vartheta(\boldsymbol{v}(E,-2,\phi)) =$

$\vartheta(\boldsymbol{k}_{-2}(E))+\pi$, we have

$$\frac{\cos\vartheta(\boldsymbol{v}(E,-\nu',\phi'))}{\cos\vartheta(\boldsymbol{v}(E,-\nu,\phi))}=(-1)^{\nu'-\nu}\frac{\cos\vartheta(\boldsymbol{k}_{-\nu'}(E))}{\cos\vartheta(\boldsymbol{k}_{-\nu}(E))}. \quad (23)$$

Then the transport time is found to be

$$\tau_{-\nu}(E)=\tau_0\frac{N_{-\nu}(E)}{N_0}\left(\frac{2N_0}{N_<(E)}\right)^2, \quad (24)$$

where $\left(\frac{2N_0}{N_<(E)}\right)^2=\frac{E_R^2+2E_RE}{E_R^2}$. Comparing this transport time for negative energies to Eq. (17) for positive energies, one can see that they share the same form.

Therefore, the nonequilibrium DF satisfying the particle number conservation requirement is

$$g_{-\nu}(E)=\left(-\frac{\partial f^0}{\partial E}\right)\boldsymbol{F}_E\cdot\left[(-1)^{\nu-1}\frac{\hbar\boldsymbol{k}_{-\nu}(E)}{m}\right]\tau_0\left(\frac{2N_0}{N_<(E)}\right)^2. \quad (25)$$

Here $N_<(E)$ is given by Eq. (5). We use the simplified notation $g_\lambda(E)$ and $g_{-\nu}(E)$ to represent the DF for brevity. It is obvious that this DF for negative energies is formally similar to that for positive energies when the latter is re-expressed as

$$g_\lambda(E)=\left(-\frac{\partial f^0}{\partial E}\right)\boldsymbol{F}_E\cdot\frac{\hbar\boldsymbol{k}_\lambda(E)}{m}\tau_0\left(\frac{2N_0}{N_>(E)}\right)^2, \quad (26)$$

except for one significant difference: the $(-1)^{\nu-1}$ factor for negative energies. This factor denotes nothing but the important fact that, for electrons with negative energy on the branch $\nu=2$, the group velocity and momentum have opposite directions [see Eq. (7) and Fig. 1].

From Eqs. (18) and (25), the out-of-equilibrium DFs in the above two energy regimes are continuous at $E=0$: $g_+(E\to0^+)=g_{-2}(E\to0^-)=0$, $g_{-1}(E\to0^-)=g_-(E\to0^+)$.

4 Electric-field- and temperature-gradient-induced spin polarization

In this section, we calculate the EISP and TISP in the Rashba model. An analytic expression for the TISP is derived, and the formula is valid even for Fermi energies near the band crossing point.

Because the nonequilibrium state is driven by the effective electric field $\boldsymbol{E}^*=\boldsymbol{E}-\frac{1}{e}\boldsymbol{\nabla}\mu$ and temperature gradient $(-\boldsymbol{\nabla}T)$, the spin density response takes the following form:

$$\langle\hat{\boldsymbol{\sigma}}\rangle_{ext}=\boldsymbol{\chi}_{\boldsymbol{E}}\cdot\boldsymbol{E}^*+\boldsymbol{\chi}_{\nabla T}\cdot(-\boldsymbol{\nabla}T). \quad (27)$$

Here the EISP coefficient $\boldsymbol{\chi}_{\boldsymbol{E}}$ and TISP coefficient $\boldsymbol{\chi}_{\nabla T}$ can be calculated from the second equation of Eq. (9), where momentum integration is performed by integrating over the energy and polar angle. By substituting the out-of-equilibrium DF, i.e., Eqs. (18) and (25), the $\boldsymbol{\chi}_{\boldsymbol{E}}$ and $\boldsymbol{\chi}_{\nabla T}$ containing contributions from both bands are given by $\boldsymbol{\chi}_{\boldsymbol{E}}(T,\mu)=\boldsymbol{\chi}_{\boldsymbol{E},+}(T,\mu)+\boldsymbol{\chi}_{\boldsymbol{E},-}(T,\mu)$:

$$\begin{aligned}\boldsymbol{\chi}_{\boldsymbol{E},+}(T,\mu)&=e\int\frac{\mathrm{d}\phi}{2\pi}\int_0^\infty\mathrm{d}EN_+(E)\left(-\frac{\partial f^0}{\partial E}\right)\\&\quad\times\boldsymbol{v}(E,+,\phi)\tau_+(E)\langle u_{\boldsymbol{k}_+(E)}|\boldsymbol{\sigma}|u_{\boldsymbol{k}_+(E)}\rangle,\\\boldsymbol{\chi}_{\boldsymbol{E},-}(T,\mu)&=e\int\frac{\mathrm{d}\phi}{2\pi}\Bigg[\int_0^\infty\mathrm{d}EN_-(E)\left(-\frac{\partial f^0}{\partial E}\right)\\&\quad\times\boldsymbol{v}(E,-,\phi)\tau_-(E)\langle u_{\boldsymbol{k}_-(E)}|\boldsymbol{\sigma}|u_{\boldsymbol{k}_-(E)}\rangle\\&\quad+\sum_\nu\int_{E_-(k_R)}^0\mathrm{d}EN_{-\nu}(E)\left(-\frac{\partial f^0}{\partial E}\right)\\&\quad\times\boldsymbol{v}(E,-\nu,\phi)\tau_{-\nu}(E)\langle u_{\boldsymbol{k}_{-\nu}(E)}|\boldsymbol{\sigma}|u_{\boldsymbol{k}_{-\nu}(E)}\rangle\Bigg], \quad (28)\end{aligned}$$

and

$$\boldsymbol{\chi}_{\nabla T}(T,\mu)=\frac{1}{e}\int_{E_-(k_R)}^\infty\mathrm{d}E(-\partial_Ef^0)\frac{E-\mu}{T}\boldsymbol{\chi}_{\boldsymbol{E}}(E). \quad (29)$$

Here and below, we use the simplified notation $\boldsymbol{\chi}_{\boldsymbol{E}}(E)$ to represent the zero-temperature EISP coefficient $\boldsymbol{\chi}_{\boldsymbol{E}}(T=0,E)$ for brevity. $\boldsymbol{\chi}_{\boldsymbol{E}}$ is a tensor and has two indices: $\boldsymbol{\chi}_{\boldsymbol{E}}(i,j)$, where i specifies the spin component, and j indicates the direction of the electric field. Owing to the isotropy, we can apply the generalized force only in the x direction for the calculation, and only $\boldsymbol{\chi}_{\boldsymbol{E}}(\hat{y},\hat{x})$ will be calculated below ($\boldsymbol{\chi}_{\boldsymbol{E}}(\hat{x},\hat{x})=0$). In addition, we will drop the indices $(\hat{y},\hat{x})$ in $\boldsymbol{\chi}_{\boldsymbol{E}}(\hat{y},\hat{x})$ for simplicity: $\chi_{\boldsymbol{E}}$.

4.1 EISP

The zero-temperature EISP for $E_F\geqslant0$ can be obtained easily from Eq. (28) as

$$\chi_{\boldsymbol{E}}(E_F\geqslant0)=e\tau_0\frac{\alpha}{\hbar}2N_0. \quad (30)$$

This result has been well-known since Edelstein presented it [7]. It is independent of the Fermi energy because the directions of spin on the inner (+) and outer (−) Fermi circles are opposite at the same polar angle ϕ, and the E_F dependence of the EISPs in the two Fermi circles cancels.

However, for Fermi energies below the band crossing point, the EISP takes the following non-Edelstein form:

$$\chi_{\boldsymbol{E}}(E_F\leqslant0)=e\tau_0\frac{\alpha}{\hbar}2N_0\left(1+\frac{2E_F}{E_R}\right). \quad (31)$$

It is linearly dependent of the Fermi energy, in contrast to the positive Fermi energy case. In the band valley,

the orientations of the spin on the inner (-2) and outer (-1) Fermi circles are parallel at the same ϕ, and the E_F dependence of the EISPs of the two Fermi circles does not cancel. Because the Fermi surface topology in the band valley differs from that above the band crossing point, the behavior of the EISPs in the two regimes also differ. $\chi_{\boldsymbol{E}}(E)$ is continuous at $E=0$. The contribution to $\chi_{\boldsymbol{E}}(0)$ comes entirely from the outer Fermi circle, $(E_F=0, k=2k_R)$, as the DOS at the band crossing point, $(E_F=0, k=0)$, is zero.

We compare Eqs. (30) and (31) to the EISP obtained by employing the constant RTA in Ref. [16]: $\chi_{\boldsymbol{E}}^{RTA}(E_F \geqslant 0) = e\tau\frac{\alpha}{\hbar}2N_0$, $\chi_{\boldsymbol{E}}^{RTA}(E_F \leqslant 0) = e\tau\frac{\alpha}{\hbar}2N_0\sqrt{1+\frac{2E_F}{E_R}}$, where τ is a constant relaxation time independent of the energy and band. For $E_F \geqslant 0$, the EISP obtained by the constant RTA has the same Edelstein form, whereas when $E_F \leqslant 0$, the constant RTA result shows a different E_F dependence from ours:

$$\begin{aligned}
&\frac{\chi_{\boldsymbol{E}}(E_F\leqslant 0)}{\chi_{\boldsymbol{E}}(0)} = 1+\frac{2E_F}{E_R},\\
&\frac{\chi_{\boldsymbol{E}}^{RTA}(E_F\leqslant 0)}{\chi_{\boldsymbol{E}}^{RTA}(0)} = \sqrt{1+\frac{2E_F}{E_R}}.
\end{aligned} \tag{32}$$

Now we calculate the spin polarization efficiency, defined as the ratio between the EISP and the driven electric-current density. The electrical conductivity for the same model has been given by [33]: $\sigma(E_F \geqslant 0) = \frac{e^2}{2\pi^2\hbar}\frac{2\pi(E_F+E_R)\tau_0}{\hbar}$, $\sigma(E_F \leqslant 0) = \frac{e^2}{2\pi^2\hbar}\frac{2\pi(E_F+E_R)\tau_0}{\hbar}\left(1+\frac{2E_F}{E_R}\right)$. Therefore, the spin polarization efficiency is given by a single expression suitable for both positive and negative Fermi energies:

$$\frac{\chi_{\boldsymbol{E}}(E_F)}{\sigma(E_F)} = \frac{\hbar k_R}{eE_R}\frac{1}{1+\frac{E_F}{E_R}}, \tag{33}$$

which increases with decreasing Fermi energy (Fig. 2). Equations (30), (31), and (33) show that when the Fermi energy lies below the band crossing point, although the EISP is reduced, higher spin polarization efficiency is achieved.

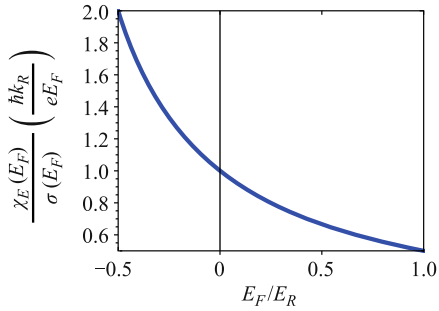

Fig. 2 Spin polarization efficiency.

4.2 TISP

We substitute $\chi_{\boldsymbol{E}}(E)$ into Eq. (29) and define

$$\begin{aligned}
&\frac{E-\mu}{k_{\rm B}T} = x, \quad \frac{\mu}{k_{\rm B}T} = -t_1, \quad \frac{E_F}{k_{\rm B}T} = -t_2,\\
&a(t_1) = \int_{t_1}^{\infty} {\rm d}x \left(-\frac{\partial f^0}{\partial x}\right) x,\\
&b(t_1) = \int_{t_1}^{\infty} {\rm d}x \left(-\frac{\partial f^0}{\partial x}\right) x^2.
\end{aligned} \tag{34}$$

Then the TISP is found to be

$$\chi_{\nabla T} = \frac{k_{\rm B}}{e}\chi_{\boldsymbol{E}}(0)\frac{2k_{\rm B}T}{E_R}\frac{\pi^2}{3}\left[1-\frac{b(t_1)-t_1a(t_1)}{\pi^2/3}\right]. \tag{35}$$

The relationship between t_2 and t_1 (i.e., the chemical potential at low temperatures) can be obtained by considering the electron density [31]:

$$\begin{aligned}
&t_2-t_1 = 0, \quad E_F \gg k_{\rm B}T,\\
&t_2-t_1 = o\left(\frac{k_{\rm B}T}{E_R}\right), \quad |E_F| \sim k_{\rm B}T,\\
&t_2-t_1 = \frac{\pi^2}{6}\frac{k_{\rm B}T}{E_R+2E_F}, \quad -E_F \gg k_{\rm B}T.
\end{aligned} \tag{36}$$

Here we consider only small thermal fluctuations, $k_{\rm B}T \ll E_R$ and $E_F+\frac{1}{2}E_R \gg k_{\rm B}T$, so that the band valley structure and Fermi surfaces survive the thermal smearing. In some new materials with a giant Rashba effect, e.g., a strongly spin–orbit-coupled 2DES near the surface of Rashba semiconductors BiTeX (X = Cl, Br, I), E_R is about 35–200 meV (in Ref. [29]). Therefore, $k_{\rm B}T \ll E_R$ and $E_F+\frac{1}{2}E_R \gg k_{\rm B}T$ can be satisfied at low temperatures (around several kelvins) for Fermi energies that are not too low.

Consequently, we can set $t_2=t_1$ in the expression for $\chi_{\nabla T}$, as Eq. (35) has already been given as $o\left(\frac{k_{\rm B}T}{E_R}\right)$:

$$\chi_{\nabla T} = \tau_0\frac{\alpha}{\hbar}2N_0k_{\rm B}\frac{\pi^2}{3}\left[1-3\frac{b(t_2)-t_2a(t_2)}{\pi^2}\right]\frac{2k_{\rm B}T}{E_R}. \tag{37}$$

This is our main result for TISP.

According to Eq. (37), $\chi_{\nabla T}$ is given in Fig. 3 in units of $\tau\frac{\alpha}{\hbar}2N_0k_{\rm B}\frac{\pi^2}{3}\frac{2k_{\rm B}T}{E_R}$. When $E_F/(k_{\rm B}T) \gtrsim 5$, $\chi_{\nabla T}$ almost vanishes. When $E_F/(k_{\rm B}T) \lesssim -5$, $\chi_{\nabla T}/\tau\frac{\alpha}{\hbar}2N_0k_{\rm B}\frac{\pi^2}{3}\frac{2k_{\rm B}T}{E_R}$ approaches a constant value of 1. In the intermediate regime, $-5 \lesssim E_F/(k_{\rm B}T) \lesssim 5$, $\chi_{\nabla T}$ decreases monotonically as $E_F/(k_{\rm B}T)$ increases.

Equation (37) can be rearranged as

$$\chi_{\nabla T} = \tau_0\frac{\alpha}{\hbar}2N_0k_{\rm B}\frac{\pi^2}{3}\frac{2|E_F|}{E_R}\left[1-\frac{b(t_2)-t_2a(t_2)}{\pi^2/3}\right]$$

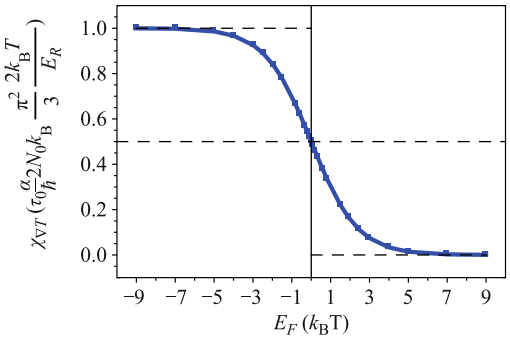

Fig. 3 Thermally induced spin polarization.

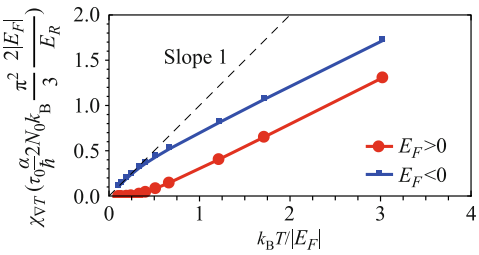

Fig. 4 The Temperature dependence of $\chi_{\nabla T}$ for positive Fermi energy (*red curve*) and negative Fermi energy (*blue curve*).

$$\cdot\frac{1}{|-t_2|}. \tag{38}$$

To clarify the temperature dependence of $\chi_{\nabla T}$, we replot $\chi_{\nabla T}$ (in units of $\tau_0\frac{\alpha}{\hbar}2N_0k_B\frac{\pi^2}{3}\frac{2|E_F|}{E_R}$) as a function of $\frac{k_BT}{|E_F|}$ ($\frac{1}{|-t_2|}$) in Fig. 4.

The figure shows that $\chi_{\nabla T}$ increases with increasing temperature. When $k_BT/E_F \lesssim 0.2$, $\chi_{\nabla T}$ fully vanishes. As k_BT/E_F continues to increase, the contribution of the band valley structure is included and dominates $\chi_{\nabla T}$, and $\chi_{\nabla T}$ is enhanced. When $k_BT/(-E_F) \lesssim 0.2$, $\chi_{\nabla T}/[\frac{\alpha}{\hbar}2N_0k_B\frac{\pi^2}{3}\frac{2(-E_F)}{E_R}]$ is almost exactly linear in $k_BT/(-E_F)$ with slope 1. When the temperature increases, not only the band valley contributes, but also the electron states above the band crossing point are included because of thermal smearing; thus, the TISP is suppressed. Moreover, when $\frac{k_BT}{|E_F|} \gg 1$, $t_2 \to 0$, $1-3\frac{b(t_2)-t_2a(t_2)}{\pi^2} \to \frac{1}{2}$, so $\chi_{\nabla T}\left(\frac{k_BT}{|E_F|} \gg 1\right) \to \chi_{\nabla T}(E_F = 0) = \tau_0\frac{\alpha}{\hbar}2N_0k_B\frac{\pi^2}{3}\frac{1}{2}\frac{2k_BT}{E_R}$, which is linear in T.

Our result for TISP is totally different from that obtained by calculating the spin–thermal current correlation function [16], which even showed that the sign of the TISP changed when the Fermi energy decreased below the band crossing point. This discrepancy may arise from the fact that in Ref. [16], only the bubble diagram for the spin–thermal current correlation function was calculated, and the vertex corrections were omitted.

5 Conclusions

In conclusion, we calculated thermoelectric responses of spin polarization in a strongly spin–orbit-coupled Rashba 2DES. By self-consistently determining the transport time, we exactly solved the Boltzmann equation when short-range impurity scattering dominates the electron relaxation process. It was shown that the EISP depends linearly on the Fermi energy when only the lower band is occupied, unlike the Edelstein behavior when both bands are occupied. Higher spin polarization efficiency is achieved when the Fermi energy lies below the band crossing point. It was found that the TISP increases continuously to a saturation value as the Fermi energy decreases below the band crossing point. In addition, the TISP tends to zero at vanishing temperature.

This work may stimulate more experimental and theoretical work on electrical and thermal spin control in Rashba semiconductors BiTeX (X = Cl, Br, I) and Bi-TeX quantum wells, as well as other materials with giant Rashba spin splitting.

Acknowledgements The Work was supported by the National Natural Science Foundation of China (Grant Nos. 11274013 and 11274018) and the National Basic Research Program of China (Grant No. 2012CB921300).

Appendix A Solutions of SBE for $E > 0$

When both Rashba bands are included, the transport time can be solved self-consistently as

$$\begin{aligned}\frac{1}{\tau_\lambda(E)} &= \sum_{\lambda'} N_{\lambda'}(E)\int\frac{\mathrm{d}\phi'}{2\pi}\omega_{\lambda',\lambda}(E)\\ &\quad\times\left\{1-\frac{|\boldsymbol{v}(E,\lambda',\phi')|}{|\boldsymbol{v}(E,\lambda,\phi)|}\frac{\tau_{\lambda'}(E)}{\tau_\lambda(E)}\right.\\ &\quad\times[\cos(\vartheta(\boldsymbol{k}_\lambda(E))-\vartheta(\boldsymbol{k}'_{\lambda'}(E)))\\ &\quad\left.+\tan\vartheta(\boldsymbol{k}_\lambda(E))\sin(\vartheta(\boldsymbol{k}_\lambda(E))-\vartheta(\boldsymbol{k}'_{\lambda'}(E)))]\right\}\\ &= \sum_{\lambda'} N_{\lambda'}(E)\int\frac{\mathrm{d}\phi'}{2\pi}\omega_{\lambda',\lambda}(E)\\ &\quad\times\left[1-\frac{|\boldsymbol{v}(E,\lambda',\phi')|}{|\boldsymbol{v}(E,\lambda,\phi)|}\cos(\phi'-\phi)\frac{\tau_{\lambda'}(E)}{\tau_\lambda(E)}\right],\end{aligned} \tag{A1}$$

where we have used

$$\cos(\vartheta(\boldsymbol{k}_\lambda(E))-\vartheta(\boldsymbol{k}'_{\lambda'}(E))) = \cos(\phi'-\phi), \tag{A2}$$

and the disappearance of the $\tan\vartheta(\boldsymbol{k}_\lambda(E))$ term makes the single isotropic transport time solution valid. Performing the angle integration in Eq. (A1) yields two al-

gebraic equations for τ_+ and τ_-. The solution is just Eq. (18), which has also been found [15] by employing Trushin's ansatz [34]. This ansatz was introduced in the anisotropic Rashba–Dresselhaus model in the presence of an electric field alone, whereas our approach is based on a simple physical picture of the isotropic transport time on constant energy surfaces.

This result differs from the modified relaxation time approximation (MRTA) solution for isotropic multiband systems (the MRTA is discussed in detail in Refs. [35] and [36]):

$$g_l^{MRTA} = \left(-\frac{\partial f^0}{\partial E_l}\right) \boldsymbol{F}_l \cdot \boldsymbol{v}_l \tau_l^{MRTA}, \tag{A3}$$

where

$$\frac{1}{\tau_l^{MRTA}} = \sum_{l'} \omega_{l',l} \left[1 - \frac{|\boldsymbol{v}_{l'}|}{|\boldsymbol{v}_l|} \cos(\vartheta(\boldsymbol{v}_l) - \vartheta(\boldsymbol{v}_{l'}))\right]. \tag{A4}$$

This MRTA solution just makes sense as an approximate solution for spin–orbit-coupled multiband isotropic transport, because if one substitutes the above g_l^{MRTA} into the SBE, τ_l^{MRTA} will be given by Eq. (A1) rather than Eq. (A4). On the other hand, to obtain Eq. (A4), one needs to neglect the band dependence of τ_l^{MRTA}. This becomes clear when Eq. (A4) is compared with Eq. (A1). However, Eq. (A4) usually gives a band-dependent result, e.g., for $E > 0$:

$$\frac{\tau_\lambda^{MRTA}(E)}{\tau_0} = \frac{N_\lambda(E)}{N_0} \cdot \frac{2(E_R^2 + 2E_R E)}{E_R^2 - \lambda E_R \sqrt{E_R^2 + 2E_R E} + 4E_R E}, \tag{A5}$$

which is band-dependent and differs from the transport time. Thus, we conclude that the MRTA is not self-consistent and is inappropriate for spin–orbit-coupled multiband isotropic systems. We can further point out that, for positive energies, the result of Eq. (A4) is the same as Eq. (17) only in the zeroth order of SOC, while it differs from the latter even in the first order of SOC in the small-SOC limit. Thus, this MRTA in a Rashba 2DES cannot even be regarded as better than the constant RTA obtained by neglecting the scattering-in term directly.

Appendix B Solutions of SBE for $E_-(k_R) < E < 0$

For $E_-(k_R) < E < 0$, the SBE (10) can be expressed as

$$\begin{aligned}\boldsymbol{F}_E \cdot \boldsymbol{v}(E, -\nu, \phi) \frac{\partial f^0}{\partial E} &= -\int \frac{\mathrm{d}\phi'}{2\pi} \left(\int_0^{k_R} + \int_{k_R}^{\infty}\right) \frac{k' \mathrm{d}k'}{2\pi} \\ &\times \omega_{-\boldsymbol{k}', -\boldsymbol{k}_{-\nu}} (g_{-\boldsymbol{k}_{-\nu}} - g_{-\boldsymbol{k}'}).\end{aligned} \tag{B1}$$

We convert the momentum integration into an integration over energy. Because the scattering is elastic, we obtain

$$\begin{aligned}\boldsymbol{F}_E \cdot \boldsymbol{v}(E, -\nu, \phi) \frac{\partial f^0}{\partial E} = -\int \frac{\mathrm{d}\phi'}{2\pi} \{&N_{-2}(E) \omega_{-2,-\nu}(E) [g_{-\nu}(E, \vartheta(\boldsymbol{v}(E, -\nu, \phi))) - g_{-2}(E, \vartheta(\boldsymbol{v}(E, -2, \phi')))] \\ &+ N_{-1}(E) \omega_{-1,-\nu}(E) [g_{-\nu}(E, \vartheta(\boldsymbol{v}(E, -\nu, \phi))) - g_{-1}(E, \vartheta(\boldsymbol{v}(E, -1, \phi')))]\},\end{aligned} \tag{B2}$$

which is just Eq. (20). Substituting $|\boldsymbol{v}(E, -\nu, \phi)| = \frac{N_0}{N_{-\nu}(E)} \frac{\hbar k_{-\nu}(E)}{m}$ and Eq. (23) into Eq. (22), we obtain

$$\frac{1}{\tau_{-\nu}(E)} = \sum_{\nu'} N_{-\nu'}(E) \int \frac{\mathrm{d}\phi'}{2\pi} \omega_{-\nu',-\nu}(E) \left[1 - (-1)^{\nu'-\nu} \cos(\phi' - \phi) \frac{\tau_{-\nu'}(E)}{\tau_{-\nu}(E)}\right]. \tag{B3}$$

Performing the integration over the polar angle yields two algebraic equations ($\nu = 1, 2$). By solving these equations, the transport time is found to be that given by Eq. (24).

References

1. I. Žutić, J. Fabian, and S. Das Sarma, Spintronics: Fundamentals and applications, *Rev. Mod. Phys.* 76(2), 323 (2004)
2. W. Lai, C. Zhang, and Z. Ma, Single molecular shuttle junction: Shot noise and decoherence, *Front. Phys.* 10(1), 591 (2015)
3. G. E. W. Bauer, E. Saitoh, and B. J. van Wees, Spin caloritronics, *Nat. Mater.* 11(5), 391 (2012)
4. X. T. Jia and K. Xia, Electric and thermo spin transfer torques in Fe/Vacuum/Fe tunnel junction, *Front. Phys.* 9(6), 768 (2014)
5. J. Sinova, D. Culcer, Q. Niu, N. A. Sinitsyn, T. Jungwirth, and A. H. MacDonald, Universal intrinsic spin Hall effect, *Phys. Rev. Lett.* 92(12), 126603 (2004)
6. J. E. Hirsch, Spin Hall effect, *Phys. Rev. Lett.* 83(9), 1834 (1999)
7. V. M. Edelstein, Spin polarization of conduction electrons

induced by electric current in two-dimensional asymmetric electron systems, *Solid State Commun.* 73(3), 233 (1990)

8. E. G. Mishchenko, A. V. Shytov, and B. I. Halperin, Spin current and polarization in impure two-dimensional electron systems with spin–orbit coupling, *Phys. Rev. Lett.* 93(22), 226602 (2004)
9. C. Gorini, P. Schwab, M. Dzierzawa, and R. Raimondi, Spin polarizations and spin Hall currents in a twodimensional electron gas with magnetic impurities, *Phys. Rev. B* 78(12), 125327 (2008)
10. Z. Ma, Spin Hall effect generated by a temperature gradient and heat current in a two-dimensional electron gas, *Solid State Commun.* 150(11–12), 510 (2010)
11. H. Akera and H. Suzuura, Extrinsic spin Nernst effect in two-dimensional electron systems, *Phys. Rev. B* 87(7), 075301 (2013)
12. J. Borge, C. Gorini, and R. Raimondi, Spin thermoelectrics in a disordered Fermi gas, *Phys. Rev. B* 87(8), 085309 (2013)
13. P. E. Iglesias and J. A. Maytorena, Absence of thermospin current response of a spin–orbit-coupled two dimensional electron gas, *Phys. Rev. B* 89(15), 155432 (2014)
14. K. Tauber, M. Gradhand, D. V. Fedorov, and I. Mertig, Extrinsic spin Nernst effect from first principles, *Phys. Rev. Lett.* 109(2), 026601 (2012)
15. C. M. Wang and M. Q. Pang, Thermally induced spin polarization and thermal conductivities in a spin–orbit coupled two-dimensional electron gas, *Solid State Commun.* 150(33–34), 1509 (2010)
16. A. Dyrdał, M. Inglot, V. K. Dugaev, and J. Barnas, Thermally induced spin polarization of a two-dimensional electron gas, *Phys. Rev. B* 87(24), 245309 (2013)
17. S. Tölle, C. Gorini, and U. Eckern, Room temperature spin thermoelectrics in metallic films, *Phys. Rev. B* 90(23), 235117 (2014)
18. E. Cappelluti, C. Grimaldi, and F. Marsiglio, Topological change of the Fermi surface in low-density Rashba gases: Application to superconductivity, *Phys. Rev. Lett.* 98(16), 167002 (2007)
19. C. Grimaldi, Electron spin dynamics in impure quantum wells for arbitrary spin–orbit coupling, *Phys. Rev. B* 72(7), 075307 (2005)
20. L. Wu, J. Yang, S. Wang, P. Wei, J. Yang, W. Zhang, and L. Chen, Thermopower enhancement in quantum wells with the Rashba effect, *Appl. Phys. Lett.* 105(20), 202115 (2014)
21. C. Grimaldi, E. Cappelluti, and F. Marsiglio, Off-Fermi surface cancellation effects in spin-Hall conductivity of a two-dimensional Rashba electron gas, *Phys. Rev. B* 73, 081303(R) (2006)
22. K. Tsutsui and S. Murakami, Spin-torque efficiency enhanced by Rashba spin splitting in three dimensions, *Phys. Rev. B* 86(11), 115201 (2012)
23. J. Nitta, T. Akazaki, H. Takayanagi, and T. Enoki, Gate control of spin–orbit interaction in an inverted $In_{0.53}Ga_{0.47}As/In_{0.52}Al_{0.48}As$ heterostructure, *Phys. Rev. Lett.* 78(7), 1335 (1997)
24. S. V. Eremeev, I. A. Nechaev, Yu. M. Koroteev, P. M. Echenique, and E. V. Chulkov, Ideal two-dimensional electron systems with a giant Rashba-type spin splitting in real materials: Surfaces of Bismuth tellurohalides, *Phys. Rev. Lett.* 108(24), 246802 (2012)
25. S. V. Eremeev, I. P. Rusinov, I. A. Nechaev, and E. V. Chulkov, Rashba split surface states in BiTeBr, *New J. Phys.* 15(7), 075015 (2013)
26. G. Landolt, S. V. Eremeev, Y. M. Koroteev, B. Slomski, S. Muff, T. Neupert, M. Kobayashi, V. N. Strocov, T. Schmitt, Z. S. Aliev, M. B. Babanly, I. R. Amiraslanov, E. V. Chulkov, J. Osterwalder, and J. H. Dil, Disentanglement of surface and bulk Rashba spin splittings in noncentrosymmetric BiTeI, *Phys. Rev. Lett.* 109(11), 116403 (2012)
27. G. Landolt, S. V. Eremeev, O. E. Tereshchenko, S. Muff, B. Slomski, K. A. Kokh, M. Kobayashi, T. Schmitt, V. N. Strocov, J. Osterwalder, E. V. Chulkov, and J. Hugo Dil, Bulk and surface Rashba splitting in single termination BiTeCl, *New J. Phys.* 15(8), 085022 (2013)
28. A. Crepaldi, L. Moreschini, G. Autes, C. Tournier-Colletta, S. Moser, N. Virk, H. Berger, P. Bugnon, Y. J. Chang, K. Kern, A. Bostwick, E. Rotenberg, O. V. Yazyev, and M. Grioni, Giant ambipolar Rashba effect in the semiconductor BiTeI, *Phys. Rev. Lett.* 109(9), 096803 (2012)
29. M. Sakano, M. S. Bahramy, A. Katayama, T. Shimojima, H. Murakawa, Y. Kaneko, W. Malaeb, S. Shin, K. Ono, H. Kumigashira, R. Arita, N. Nagaosa, H. Y. Hwang, Y. Tokura, and K. Ishizaka, Strongly spin–orbit coupled two-dimensional electron gas emerging near the surface of polar semiconductors, *Phys. Rev. Lett.* 110(10), 107204 (2013)
30. I. P. Rusinov, I. A. Nechaev, S. V. Eremeev, C. Friedrich, S. Blugel, and E. V. Chulkov, Many-body effects on the Rashba-type spin splitting in bulk bismuth tellurohalides, *Phys. Rev. B* 87(20), 205103 (2013)
31. J. M. Ziman, Principles of the Theory of Solids, Cambridge: Cambridge University Press, 1972
32. N. A. Sinitsyn, Semiclassical theories of the anomalous Hall effect, *J. Phys.: Condens. Matter* 20(2), 023201 (2008)
33. C. Xiao, D. P. Li, and Z. S. Ma, Unconventional thermoelectric behaviors and enhancement of figure of merit in Rashba spintronic systems, arXiv: 1507.04237
34. M. Trushin and J. Schliemann, Anisotropic current induced spin accumulation in the two-dimensional electron gas with spin–orbit coupling, *Phys. Rev. B* 75(15), 155323 (2007)
35. K. Výborný, A. A. Kovalev, J. Sinova, and T. Jungwirth, Semiclassical framework for the calculation of transport anisotropies, *Phys. Rev. B* 79(4), 045427 (2009)
36. M. Trushin, K. Vyborny, P. Moraczewski, A. A. Kovalev, J. Schliemann, and T. Jungwirth, Anisotropic magnetoresistance of spin–orbit coupled carriers scattered from polarized magnetic impurities, *Phys. Rev. B* 80(13), 134405 (2009)